Rhim et al. Nano Convergence 20152:10
DOI 10.1186/s40580-014-0041-3

Nano Convergence
a SpringerOpen Journal

REVIEW Open Access

Radionuclide-labeled nanostructures for *In Vivo* imaging of cancer

Won-Kyu Rhim[1†], Minho Kim[1†], Kevin L Hartman[1], Keon Wook Kang[2] and Jwa-Min Nam[1*]

Abstract

Molecular imaging plays an important role in the non-invasive diagnosis and the guiding or monitoring of disease treatment. Different imaging modalities have been developed, and each method possesses unique strengths. While a variety of molecules have been used previously in nuclear imaging, the exceptional properties of nanostructures in recent research enable the deployment of accurate and efficient diagnostic agents using radionuclide-nanostructures. This review focuses on the radionuclide labeling strategies of various nanostructures and their applications for multimodality tumor imaging.

Keywords: Nanoprobe; Molecular imaging; Radionuclide; Positron emission tomography (PET); Single photon emission computed tomography (SPECT); Multimodality

1 Introduction

Over the past decade, molecular imaging has emerged and expanded rapidly due to its great potential for understanding biological reactions, detecting diseases in early stages, providing accurate diagnosis, and visualizing pathologic processes and cellular functions at the molecular and cellular level without perturbing the living organism [1-5]. Several types of tools have been developed for molecular imaging, such as magnetic resonance imaging (MRI), computed tomography (CT), positron emission tomography (PET), single photon emission computed tomography (SPECT), contrast enhanced ultrasound (CEUS), and optical fluorescence [6]. PET, SPECT, and other radionuclide-based imaging methods have been extensively used in biomedical and clinical fields due to their excellent features of high sensitivity, easy quantitation, and strong penetration through tissue [7-10].

In the case of nuclear molecular imaging tools (PET and SPECT), radionuclide-labeled substances are used as contrast agents. Generally, radionuclides are linked via a chelating agent to targeting components, such as antibodies, antibody fragments, peptides, proteins, oligonucleotides, or receptor ligands [11-16]. Recently, nanoparticles have been noted as a remarkable radionuclide carrier due to their chemical and biological stability, high loading capacity, noteworthy physicochemical properties, and practically limitless surface-functionalization [17]. Although several functionalization methods using chelating agents have been suggested and developed [18-24], those methods have numerous limitations for nuclear molecular imaging because the radionuclides originally incorporated with chelating agents can detach from those molecules *in vivo* [25-27]. These instabilities may induce false target detection, which decreases the accuracy of diagnostic information. Therefore, functionalization methods free of chelating agents have been sought recently as a way to overcome those drawbacks [28-32].

For practical purposes, molecular imaging tools are not sufficient by themselves due to their inherent limitations. For example, while the imaging modes PET and SPECT are highly sensitive, quantitative, and show good tissue penetration depth, they are limited by their low spatial resolution [6]. Therefore, the combination of two or more molecular imaging tools, otherwise known as multimodality imaging, should be used to overcome the deficiencies of individual imaging modes to ensure the accuracy of molecular imaging applications. Moreover, the unique properties of nanostructures can be used to their advantage to lessen the amount of radionuclide used and maximize the benefits of multimodality imaging.

* Correspondence: jmnam@snu.ac.kr
†Equal contributors
[1]Department of Chemistry, Seoul National University, Seoul 151-747, Republic of Korea
Full list of author information is available at the end of the article

In this review paper, we will present radionuclide labeling strategies on various nanostructures and their applications of multimodality tumor imaging.

2 Review

Molecular imaging of living organisms involves the visualization of biological processes and cellular functions at the molecular and cellular levels [33]. This can be used for diagnosis of diseases such as cancer, neurological, and cardiovascular conditions without any invasion to the living organism [1,3]. In general, the field of molecular imaging for clinical use includes magnetic resonance imaging (MRI), computed tomography (CT), positron emission tomography (PET), single photon emission computed tomography (SPECT), contrast enhanced ultrasound (CEUS), and optical fluorescence. Taking into account sensitivity, spatial resolution, and temporal depth resolution, each molecular imaging tool has different sets of capabilities [6]. For instance, the lack of penetration depth limit of PET and SPECT, coupled with their high sensitivity (down to the picomolar range) and quantitative abilities make them powerful tools for *in vivo* imaging [34]. Molecular imaging includes the administration of imaging probes and the detection of specific signals produced from the probes. In PET, the system detects pairs of gamma rays emitted by positron-emitting radionuclides [35]. Positrons interact with nearby electrons at a distance of ~1 mm, transmutating to generate and emit 511 keV gamma photons. To enable this process, various positron-emitting isotopes are available for PET imaging. Among them, ^{18}F and ^{64}Cu are attractive radionuclides for site-specific imaging. Fluorodeoxyglucose (FDG) is the most commonly used radiotracer for tumor-targeted imaging. It is taken up by cells with a high need for glucose such as those in the heart, brain, and tumor [36]. ^{64}Cu is also a good candidate to be labeled onto biomolecules like antibodies and peptides due to its proper decay half-life, relatively low energy, and commercial availability [2]. In SPECT, computer-generated three-dimensional images of radioactive tracers are produced by detecting single gamma ray photons [37]. A single gamma photon is generated when each radionuclide decays from a higher energy state to a lower state. SPECT imaging uses gamma emitting radioisotopes such as ^{93m}Tc, ^{111}In, ^{123}I, and ^{131}I.

Nanostructures, which range in size from 1 to 100 nm, have a high surface area to volume ratio and strong, controllable binding capacity for specific molecules. This allows for varied surface modification and the multivalent binding of targets, which suggests new applications in molecular imaging and nanomedicine [38-48]. While active targeting is advantageous, the most important factor of nanostructure development for bioimaging is the enhanced permeability and retention (EPR) effect due to the leakage of neovasculature in tumor. The EPR effect is the property that only molecules and particles of specific sizes accumulate in tumor tissues. The effect is due to the abnormal angiogenesis caused by various growth factor stimulation in tumor tissues [49]. Nanostructures of 100 nm in diameter can be optimum candidates for maximizing the EPR effect *in vivo*. Moreover, modifying surface charge and flexibility allow control of nanostructure biodistribution [43,46,50]. For nanoparticles with different surface properties and multifunctional groups, proper isotope and radiolabeling methods need to be considered carefully for optimized imaging outcome. After labeling with a radionuclide, functionalized nanostructures can serve as good candidates for molecular imaging probes (PET or SPECT). The two major strategies for labeling nuclides onto nanostructures depend on whether or not chelating agents are used. The chelation-free labeling methods include self-radioactive nanostructures and the direct attachment of radionuclides onto the nanostructures, which both utilize specific interactions between the radioisotope and the nanostructure. In the earlier examples of this work, radionuclides (radioisotopes), which are used as radiotracers for nuclear molecular imaging (PET or SPECT), were combined with nanoparticles, including gold nanoparticles [18,19,51], carbon-based nanomaterials [20-22,52], and quantum dots [53,54], through a chelating agent, such as DOTA, NOTA, and others [55]. Moreover, chloramine T can act as an oxidizing agent in the synthesis of the Bolton-Hunter reagent to label radioactive iodine [56]. Although many chelating agents were tested to label radioisotopes more efficiently, DOTA is the most attractive candidate due to its FDA approval for human application.

2.1 Chelating agent-mediated nanostructures

2.1.1 Gold nanostructures

Colloidal gold nanoparticles (AuNPs) are attractive candidates as imaging probes because of their low cytotoxicity in a variety of cell and animal models [32,57-60]. Moreover, AuNPs can be easily modified with biomolecules (e.g., DNA and peptides) via thiol-Au bonds, and many other functional ligands can also be incorporated. Xie et al. reported a ^{64}Cu-chelated gold nanoshell (AuNS) structure for *in vivo* PET imaging and photothermal therapy [18]. For this, the bifunctional chelating agent p-NH2-Bn-DOTA (S-2-(4-aminobenzyl)-1,4,7,10-tetraazacyclododecane tetraacetic acid) was conjugated to bifunctional OPSS-PEG2K-NHS (opyridyldisulfide-polyethylene glycol 2000-N-hydroxysuccinimide) (Figure 1(a)). About 90% of the resulting ^{64}Cu-chelated AuNS was stable for 3 hrs in PBS solution or serum, and showed accumulation in the squamous cell carcinoma region by the EPR effect. In

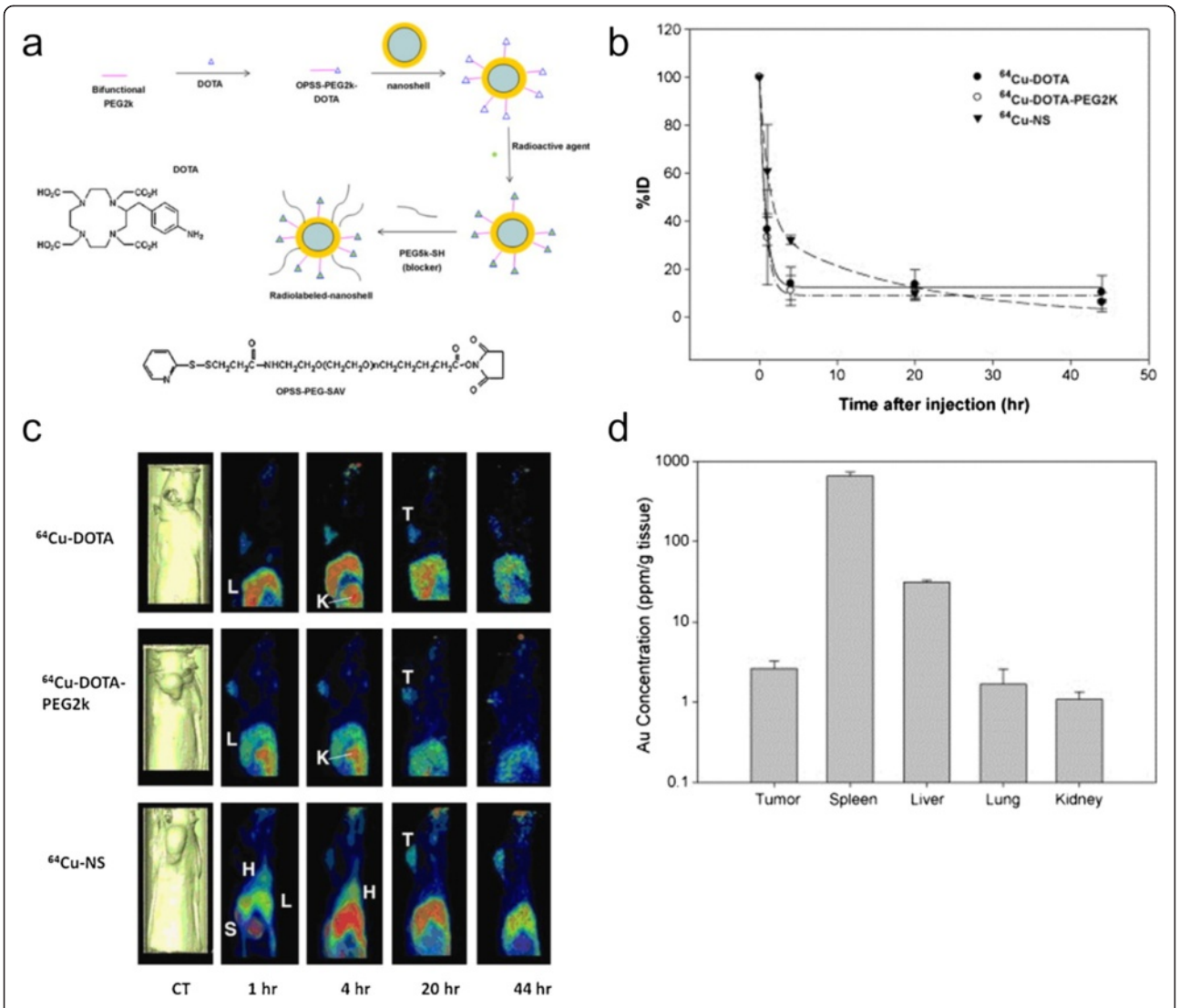

Figure 1 ***In vivo*** **PET imaging of radiolabeled gold nanoshell structure with tumor. (a)** Synthesis of radiolabeled AuNS conjugates. **(b)** Pharmacokinetics, expressed as the percentage of the injected dose (%ID), of ^{64}Cu-DOTA, ^{64}Cu-DOTA-PEG2K, and ^{64}Cu-NS at 0, 4, 20, and 44 h p.i. Significantly different pharmacokinetics between ^{64}Cu-NS and the two controls are evident at 4 h p.i. ($p < 0.05$). **(c)** PET images at different time points with three different probes. (^{64}Cu-DOTA, ^{64}Cu-DOTA-PEG2K, and ^{64}Cu-NS) **(d)** Biodistribution of ^{64}Cu-NS in several major organs. (Adapted with permission from Ref. 18. Copyright (2010) Elsevier).

pharmacokinetics studies, the half-life of ^{64}Cu-NS (12.76 hrs), was significantly longer than the half-lives of the ^{64}Cu-DOTA and ^{64}Cu-DOTA-PEG2K controls (0.54 and 0.52 hrs, respectively). As shown in Figure 1(b), statistical analysis proved that ^{64}Cu-NS had a much higher remaining ratio in the blood at 4 hrs post-injection (p.i.) than the two controls ($32.1 \pm 1.8\%$ ID vs. 13.9 ± 6.8 and $11.0 \pm 6.2\%$ ID; $p < 0.05$) (Figure 1(c,d)). Yucai et al. furthermore reported a ^{64}Cu-labeled DOTA-PEG-Au nanocage (^{64}Cu-DOTA-PEG-AuNC) for simultaneous *in vivo* tumor targeted PET imaging and pharmacokinetics [19]. AuNCs have effective photothermal translation activity, capable of converting light into heat and increasing the local temperature. Therefore, AuNCs can act as a photothermal therapeutic agent while its properties as an imaging agent allows simultaneous monitoring of its biodistribution. DOTA was conjugated onto the AuNC surface using an NH_2-modified PEG molecule for labeling radionuclide as a PET imaging agent. The NH_2 groups were then coupled with DOTA-NHS-ester through an amide reaction via an NHS-activated ester, followed by chelation with ^{64}Cu ions. ^{64}Cu-DOTA-PEG-AuNCs showed 81.5% stability following a 24 hr incubation in serum. Due to the reduction in size and surface charge, the 30 nm diameter ^{64}Cu-DOTA-PEG-AuNCs showed improved *in vivo* pharmacokinetics with decreased RES system uptake and enhanced blood circulation compared to the 55 nm samples.

2.1.2 Carbon nanostructures

Due to their unique geometric, chemical, and physical properties, carbon nanotubes are promising candidates for nanomedicine [61-64]. SWNT can be non-covalently functionalized with phospholipid-PEG for sustained solubility and stability in human serum environments [20]. The termini of PEG on the nanotube can be furthermore conjugated to both DOTA and integrin αvβ3, with the integrin targeting the RGD (arginine-glycine-aspartic acid) peptide for ^{64}Cu labeling and tumor imaging. Liu et al. found that SWNT chelated with ^{64}Cu in this way showed high tumor accumulation over long periods (~24 hrs).

Graphene oxide (GO) is a type of planar carbon sheet that has a great potential in nanomedicine due to its interesting properties arising from the combination of an ultrahigh surface area with a modifiable planar surface chemistry [65,66]. Though toxic in some cases, the biocompatibility of graphene oxide is dependent on the functional groups displayed [67]. For example, polyethylene glycol (PEG) functionalized GO can be excreted through the urinary tract, without inducing cytotoxicity [68]. Hong et al. developed ^{66}Ga and ^{64}Cu-chelated GO for tumor vasculature imaging [21,69]. The researchers used 1,4,7-triazacyclononane-1,4,7-triacetic acid (NOTA) for chelating both ^{66}Ga and ^{64}Cu. NOTA and TRC 105 (antibody binding to CD105) were covalently conjugated to agraphene oxide sheet consisting of six-arm branched PEG molecules on the surface (Figure 2 (a)). More than 90% of labeled ^{66}Ga and ^{64}Cu remained on the GO conjugates during a 48 hrs incubation in serum conditions (Figure 2(b)). Efficient tumor uptake of radiolabeled-NOTA-GO-TRC105 occurred with a clear visualization at early time points and a stability over 48 hrs (Figure 2(c,d)). Cornelissen et al. used doxorubicin and ^{111}In-loadedgraphene oxide (GO) for tumor targeted SPECT imaging and therapy [22]. Different from Hong et al., they labeled ^{111}In using π-π stacked benzyl-DTPA onto GO. The ^{111}In achieved a labeling yield of 98% and only less than 5% of chelated ^{111}In was lost by transchelation to serum proteins during serum incubation. ^{111}In-labeled NGO-trastuzumab constructs (which consisted of an antibody against HER2) were shown to target HER2 receptors with high specificity.

2.1.3 Lipid nanostructures

Liposomes are clinically well-established drug delivery vehicles with properties including biocompatibility, high drug-to-carrier ratios, and straightforward drug encapsulation capability [70-73]. The polar and non-polar domains of the molecules comprising the liposome structure allow the stable encapsulation of both hydrophilic and hydrophobic agents. The incorporation of hydrophilic polyethylene glycol on the surface of liposomes further improves their properties of low opsonization and long circulation time [43]. Seo et al. reported a novel ^{64}Cu labeling method for liposomes [23]. The researchers conjugated a ^{64}Cu specific chelating agent, 6-[*p*-(bromoacetamido) benzyl]-1,4,8,11-tetraazacyclotetradecane-*N*,*N*',*N*'',*N*'''-tetraacetic acid (BAT) to an artificial lipid molecule to form a BAT-PEG-lipid, followed by successfully incorporating ^{64}Cu into liposomes at pH 5. About 88% of ^{64}Cu was encapsulated into the liposomes over the course of a 48 hr serum incubation. Different from the above method, Petersen et al. demonstrated remote loading of ^{64}Cu into a liposome using a novel inophore, 2-hydroxyquinoline [24]. By remote loading, the radionuclide becomes entrapped in the aqueous core of the liposome, rather than on the surface. For the remote loading mechanism, 2-hydroxyquinoline carries ^{64}Cu across the lipid membrane to the aqueous portion of liposome, followed by chelation into pre-encapsulating DOTA (Figure 3(a)). Using this technique, the researchers achieved very efficient loading (95.5%) and retention stability (>99%), which shows the ^{64}Cu-liposomes to be promising PET imaging agents. This method provides maximized and stable ^{64}Cu labeling efficiency. PEG conjugated liposomes can circulate for an extended time and are able to accumulate in tumor regions through the EPR effect. The ^{64}Cu-liposomes remained in the blood-pool for over 24 hrs. The ^{64}Cu-liposome activity at the tumor site increased over the 24 hr time period post injection. This result means that the number of ^{64}Cu-liposomes delivered to the tumors continues to accumulate as long as liposomes are circulating in the blood stream (Figure 3(b)).

2.2 Chelating agent-freenanostructures

2.2.1 The need for labeling strategies free of chelating agents

Although various chelating agent-mediated radioisotope labeled nanoprobes have been suggested for nuclear molecular imaging and pharmacokinetics, chelating agent-mediated functionalization methods have several limitations for nanoparticles used *in vivo* [28]. Firstly, the functionalized radionuclides using chelating agents at the surface of nanoparticles can induce the change of intrinsic surface properties of nanoparticles, such as surface charge, polarity, and degree of hydrophobicity. Basically, the physicochemical properties of nanoparticles are strongly affected by their surface conditions [74], and therefore, chelating agent-functionalized nanoparticles may show different biodistributions or pharmacokinetic properties than compared to non-functionalized nanoparticles. Secondly, radionuclides incorporated with a chelating agent may be influenced by harsh conditions *in vivo*, resulting in the detachment of radionuclides during circulation or their replacement by biological substances due to protein

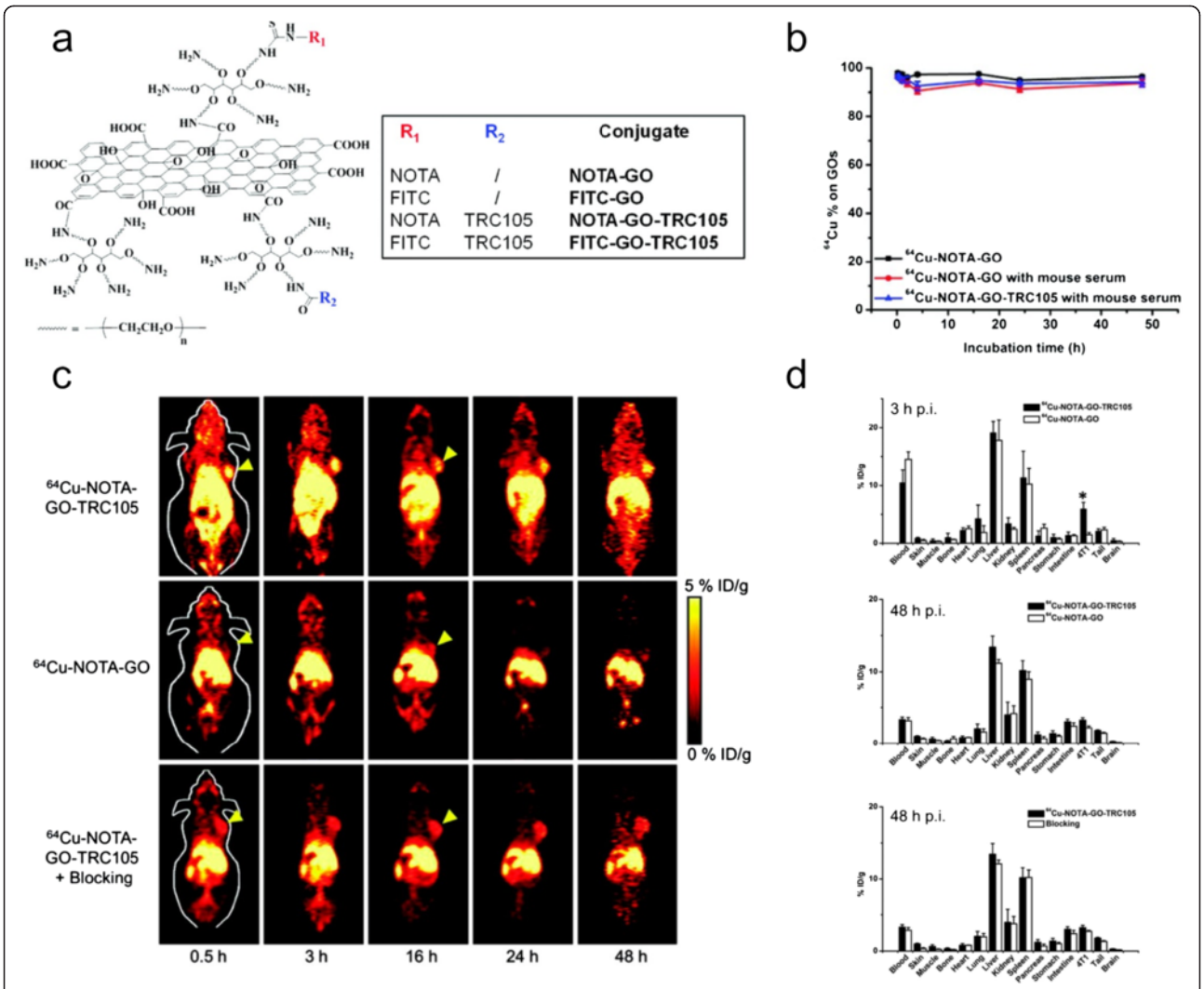

Figure 2 ***In vivo*** **targeting and PET imaging using** ^{64}**Cu-labeled nano-graphene. (a)** Schematic representation of conjugated nano-graphene. **(b)** Serum stability test of ^{64}Cu-labeled nano-graphene shows that the vast majority of ^{64}Cu remains intact on the GO after incubation in complete mouse serum at 37°C for 48 hrs. **(c)** *In vivo* PET/CT imaging of ^{64}Cu-labeled GO conjugates in 4 T1 murine breast tumor-bearing mice. Serial coronal PET images of 4 T1 tumor-bearing mice at different time points post injection (p.i.) of ^{64}Cu-NOTA-GO-TRC105, ^{64}Cu-NOTA-GO, or ^{64}Cu-NOTA-GO-TRC105 after a preinjected blocking dose of TRC105. Tumors are indicated by arrowheads. **(d)** Biodistribution studies in 4 T1 tumor-bearing mice. Biodistribution of ^{64}Cu-NOTA-GO-TRC105 and ^{64}Cu-NOTA-GO in 4 T1 tumor-bearing mice at 3 hrs and 48 hrs postinjection; $*p < 0.05$. Biodistribution of ^{64}Cu-NOTA-GO-TRC105 and ^{64}Cu-NOTA-GO-TRC105 after a blocking dose of TRC105 (denoted as blocking) in 4 T1 tumor-bearing mice at 48 h p.i. (Adapted with permission from Ref. 21. Copyright (2012) American Chemical Society).

transchelation or dehalogenation [25-27]. Accordingly, these instabilities of radionuclide-chelating agent complexes decrease the accuracy of pharmacokinetics and diagnosis data [75]. To avoid these disadvantages, researchers have been developing labeling strategies free of chelating agents. One of these studies, by Gibson et al., carried out direct radiolabelling using cyclotron accelerators to incorporate radionuclides into nanomaterials directly [76]. However, this direct incorporation method, which used neutron bombardment to generate high energy radiation, damaged the nanomaterials by causing them to aggregate.

2.2.2 Radio-labeled nanostructures free of chelating agents

Recently, nanoprobes free of chelating agents have been reported for nuclear molecular imaging [28-32]. To synthesize these, researchers have created self-radioactive nanoparticle probes using radioisotopes of metal atoms, such as ^{64}Cu or ^{198}Au, or by directly attaching radioisotopes, e.g. ^{125}I, onto the metal nanoparticle surface without a chelating agent. For example, Zhou et al. synthesized ~11 nm diameter [^{64}Cu]CuS nanoparticles for micro-PET/CT imaging and as a photothermal coupling agent for photothermal ablation, without the use of chelating agents [28] (Figure 4(a-c)). The [^{64}Cu]CuS

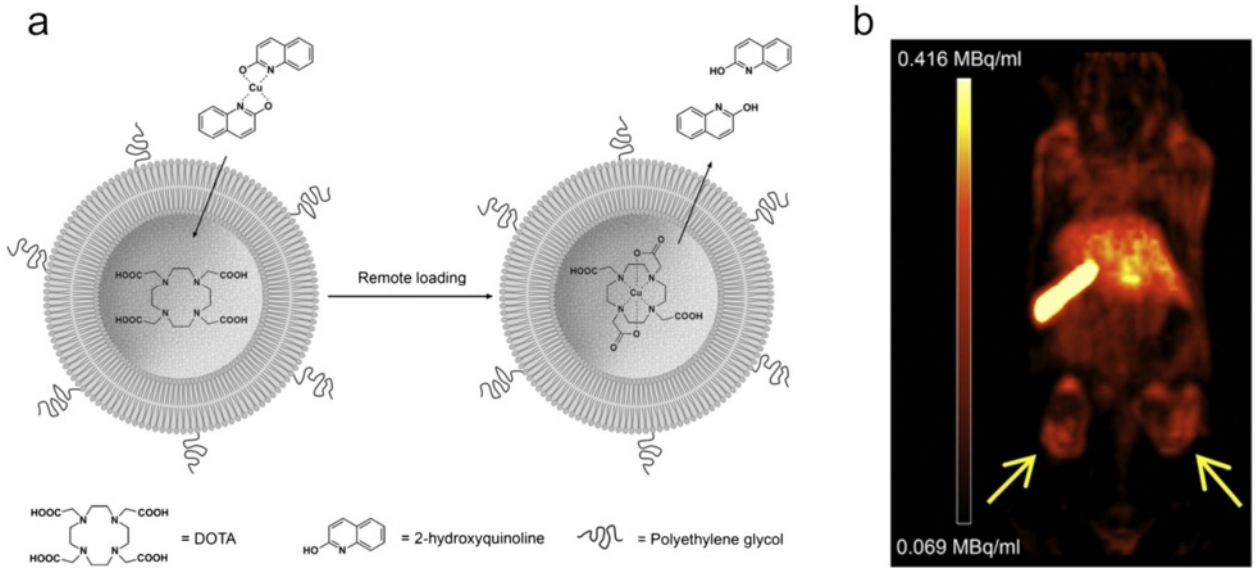

Figure 3 ^{64}Cu loaded liposome for tumor imaging using PET. (a) Remote loading of ^{64}Cu into preformed liposomes using an ionophore, 2-hydroxyquinoline. Over 99% of encapsulation efficiency was obtained with size exclusion chromatography after a remote loading method. **(b)** Coronal PET image 24 hrs post-injection of ^{64}Cu-liposomes into a mouse bearing colon adenocarcinoma (marked with arrows) on right and left flank. (Adapted with permission from Ref. 24. Copyright (2011) Elsevier).

nanoparticles, following surface PEG functionalization, showed high radiolabeling efficiency and stability in PBS or serum environments. These [^{64}Cu]CuS nanoparticles also showed high uptake in U87 human glioblastoma (U87MG) xenografts through enhanced permeability and retention effects. Furthermore, the [^{64}Cu]CuS nanoparticles strongly absorbed near-infrared (NIR) radiation (with a peak adsorption at 930 nm), and thus, they could be applied to the photothermal ablation of U87MG tumor cells upon exposure to NIR light. Therefore, these unique properties, such as small diameter, incorporation of ^{64}Cu as a radiotracer, high radiolabeling efficiency, excellent stability, and strong NIR absorption, are ideally useful for multifunctional molecular imaging and therapy. Similarly, Black et al. synthesized the radioactive ^{198}Au-doped nanostructures by directly incorporating radioactive ^{198}Au isotopes with non-radioactive ^{197}Au atoms during synthesis [29]. To use nanoparticles for*in vivo* theragnosis, the *in vivo* properties of nanoparticles including biodistribution, tumor uptake, and intratumoral distribution should be investigated and analyzed accurately. Since the *in vivo* properties of nanoparticles depend on their physicochemical characteristics including geometry, Black et al. synthesized four differently-shaped nanostructures: nanospheres, nanodisks, nanorods, and cubic nanocages, with similar sizes to confirm the shape-dependent behavior of nanoparticles using a murine EMT6 breast cancer model. They found that ^{198}Au-incorporated nanospheres showed optimal behavior with the best blood circulation, the lowest clearance by the reticuloendothelial system (RES), and the highest tumor uptake. These ^{198}Au-incorporated nanostructures have a great potential for *in vivo* molecular imaging compared to the disadvantages of radioactive nanomaterials made with chelating agents. Lately, the radioactive ^{64}Cu-alloyed [30] or ^{64}Cu-integrated [31] Au nanoparticles were synthesized for improving radiolabel stability and diagnostic accuracy, as well as PET imaging guided photothermal cancer therapy. Unlike self-radioactive nanoparticles composed of radioisotopes, Kim et al. synthesized cyclic RGD-PEGylated Au nanoparticle probes with surface conjugated radioactive ^{125}I for tumor targeting and SPECT/CT [32] (Figure 4(d-f)). The surface conjugation of ^{125}I works by the high affinity binding between the iodine ion and the Au surface [17,77-79]. This simple labeling chemistry provided high stability for ~20 hrs in serum or under various pH and high salt conditions with tumor-specific targeting for $\alpha_v\beta_3$ integrin expressing tumor cells via $\alpha_v\beta_3$-receptor-mediated endocytosis. Importantly, the ^{125}I-labeled cRGD-PEG-Au nanoprobes could target the tumor site only 10 min. after intravenous injection as observed by SPECT/CT imaging, and could be excreted from the body by renal clearance without any sign of toxicity.

2.3 Radionuclide-labeled nanostructures for multimodality tumor imaging

Generally, molecular imaging tools, such as positron emission tomography (PET), single photon emission

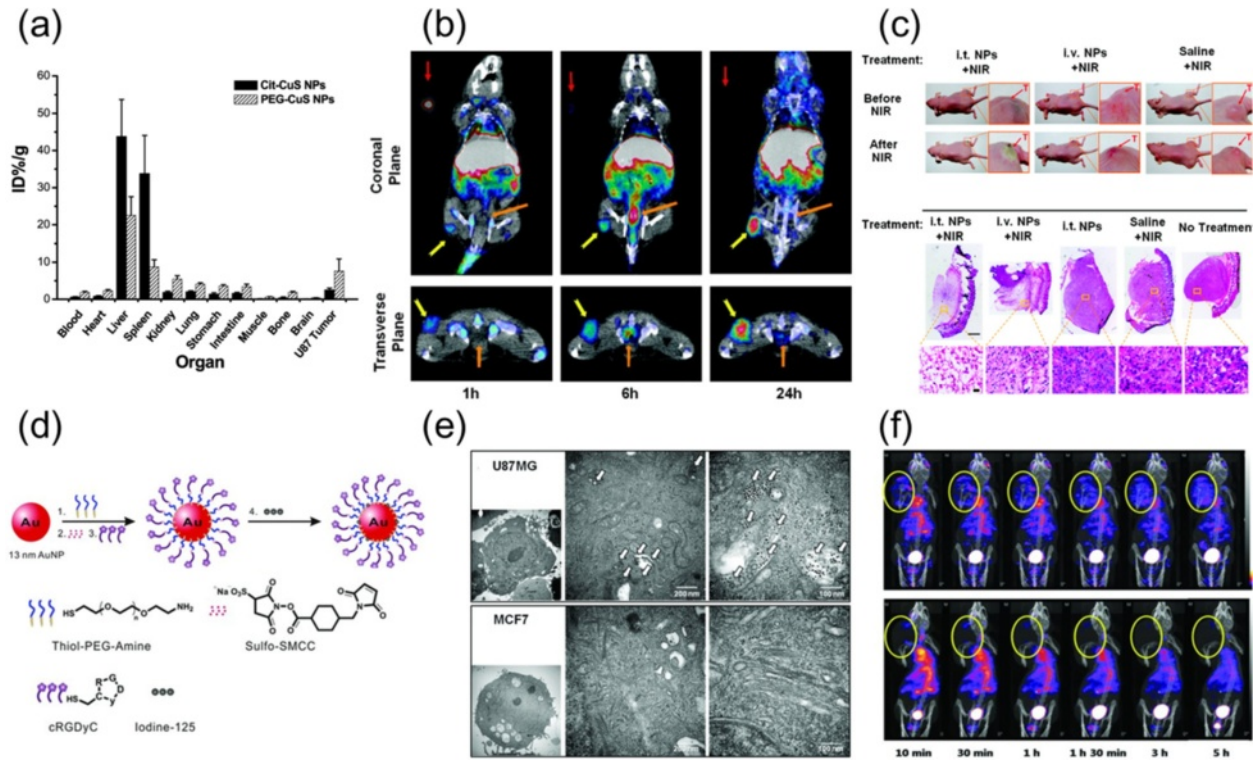

Figure 4 Chelator-free nanoprobes for nuclear molecular imaging. (a) Biodistribution of Cit-CuS NPs (n = 5) and PEG-CuS NPs (n = 5) at 24 h after i.v. injection in tumor-bearing mice. **(b)** Micro-PET/CT images of tumor-bearing nude mice acquired at 1, 6, and 24 h after i.v. injection of PEG-[^{64}Cu]CuS NPs. Yellow arrow = tumor; orange arrow = bladder, red arrow = standard. **(c)** Photographs of mice bearing subcutaneous U87 tumor before and at 24 h after NIR laser irradiation (upper panel). Representative microphotographs of tumors removed 24 h after NIR laser treatment (lower panel). Abbreviations: Cit-CuS NPs = citrate-coated CuS nanoparticles; PEG-CuS NPs = PEG-coated CuS nanoparticles; i.v. = intravenous; NIR = near-infrared. **(d)** Synthesis of cyclic RGD-PEGylated-AuNP probes labeled with radioactive iodine-125. **(e)** TEM images of cellular uptake after treated with ^{125}I-cRP-AuNPs, U87MG cells (upper panel) and MCF-7 cells (lower panel). Arrows indicate cellular uptake of ^{125}I-cRP-AuNPs in cells. **(f)** Small-animal SPECT/CT of ^{125}I-cRP-AuNPs (upper panel), and cold-form-blocked ^{125}I-cRP-AuNPs (lower panel) in nude mice bearing U87MG tumors xenografts after injection through tail vein. Yellow circles indicates tumor region (a-c adapted with permission from ref. 28. Copyright (2010) American Chemical Society & d-f adapted with permission from ref. 32. Copyright (2011) Wiley).

computed tomography (SPECT), magnetic resonance imaging (MRI), contrast-enhanced ultrasound (CEUS), and optical fluorescence, have intrinsic advantages and drawbacks simultaneously for accurate tumor imaging. For example, PET and SPECT are powerful imaging tools due to their high sensitivity, quantitative nature, and lack of a penetration limit, however, they are not perfect for single modality because of their low spatial resolution [6]. MRI enables morphological and functional imaging with no penetration limit and a high spatial resolution, however, it is limited by its low sensitivity. Optical fluorescence is widely used for molecular imaging given its low expense and high sensitivity, however, it also has several drawbacks, such as low spatial resolution, limited penetration, photobleaching, and autofluorescent emission from tissues and biomolecules. With such a wide range of capabilities, molecular imaging tools should be combined to enhance overall image quality.

2.3.1 PET(SPECT)/MR imaging

MRI is the most widely used non-invasive diagnostic technique based on the interaction of protons with surrounding molecules in the target tissue [80]. MRI provides several advantages, including high temporal and spatial resolution, soft tissue contrast, and the absence of ionizing radiation, which radionuclide-based imaging techniques, such as PET and SPECT, cannot achieve. However, MRI is limited by its low sensitivity and long acquisition time compared to PET and SPECT. Thus, as complementary techniques, PET (or SPECT) and MRI can be combined to overcome their individual limitations. The most commonly used nanoparticle-based MRI contrast agents are superparamagnetic iron oxide nanoparticles (SPIONPs), which are composed of Fe^{3+} and Fe^{2+} [81]. Usually, radionuclides are conjugated to iron oxide nanoparticles (IONPs) using chelating agents on the surface of IONPs for simultaneous dual-modal imaging techniques including PET and MRI. Lee et al. synthesized

DOTA chelating agent-mediated ^{64}Cu-labeled iron oxide nanoprobes with RGD peptide as a targeting moiety for $\alpha_v\beta_3$ integrin over-expressed U87MG tumor cells to apply PET/MR dual-modal imaging [82] (Figure 5). These probes were polyaspartic acid (PASP)-coated IO (PASP-IO) nanoparticles with a core size of 5 nm and a hydrodynamic diameter of 45 ± 10 nm, and the saturation magnetization of PASP-IO nanoparticles was about 117 emu/g of iron. With RGD conjugation, displacement competitive binding assays showed that these RGD-PASP-IO assemblies could bind specifically to integrin $\alpha_v\beta_3$ *in vitro*. Furthermore, small-animal PET, T_2-weighted MRI, and histologic analysis showed integrin-specific delivery of conjugated RGD-PASP-IO nanoparticles and prominent reticuloendothelial system (RES) uptake. Instead of ^{64}Cu, Choi et al. labeled ^{124}I on the surface of albumin-coated magnetic nanoparticles composed of $MnFe_2O_4$ via the tyrosine residue in the albumin. These probes were used for dual-modality PET/MR imaging [83]. Unlike PET/MR dual-modal imaging, Misri et al. synthesized dual-modal imaging probes for SPECT/MR by conjugating ^{111}In labeled antimesothelin antibody (mAbMB) to SPIONPs [84].

2.3.2 PET(SPECT)/optical imaging

Optical fluorescence, especially near-infrared fluorescence (NIRF) imaging technique, is most widely used for molecular imaging due to its high sensitivity, rapid scanning time with relatively inexpensive imaging instruments, and low risk to living organisms as it uses nonionizing rather than ionizing radiation. However, this imaging technique suffers from low tissue penetration, leading to poor quantification [6]. By combining fluorescence with radionuclide-based imaging techniques (PET or SPECT),

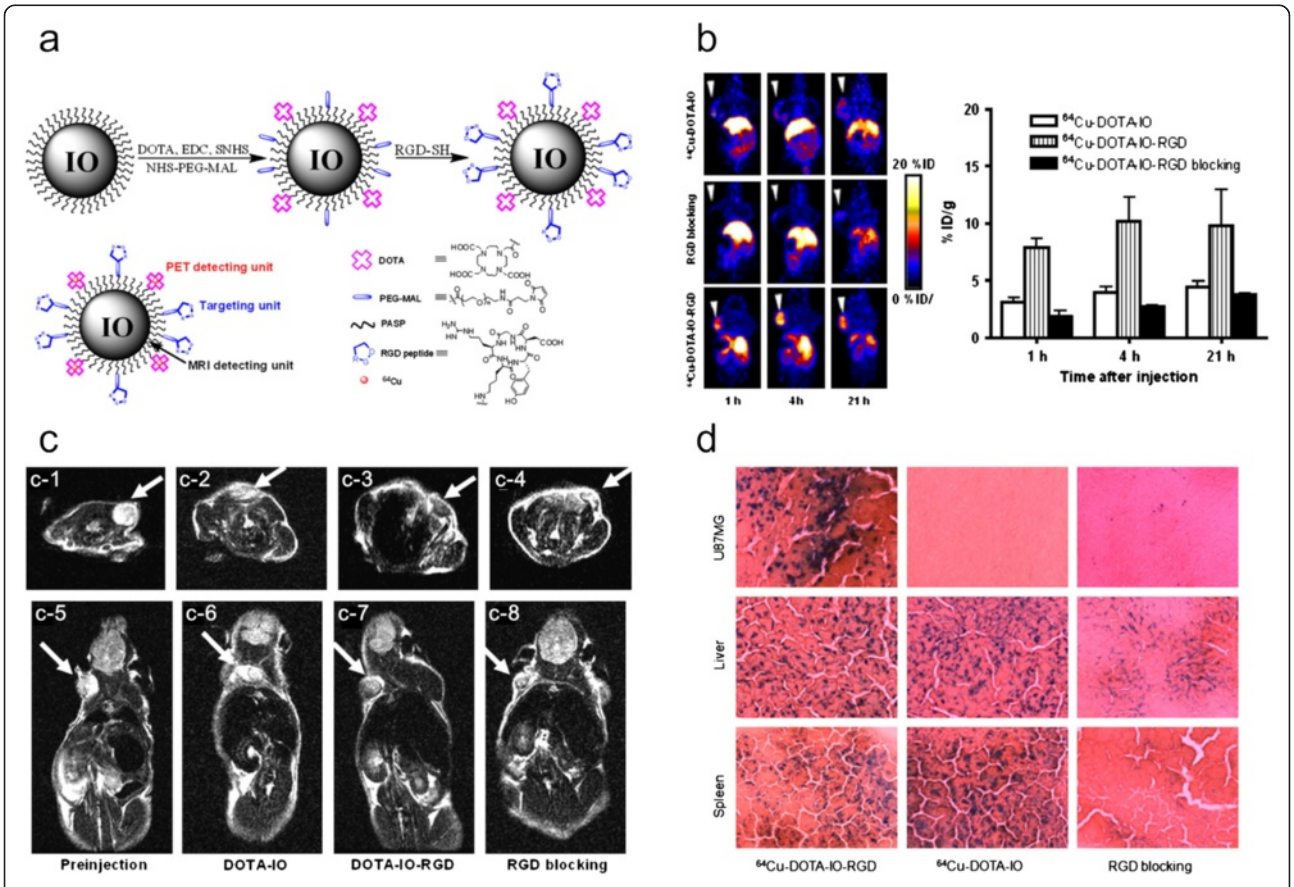

Figure 5 PET(SPECT)/MR imaging. (a) Preparation of PET/MRI dual-modality probe DOTA-IO-RGD. DOTA = 1,4,7,10-tetraazacyclododecane-*N*,*N*′,*N*″,*N*‴-tetraacetic acid; IO = Iron Oxide; RGD = arginine-glycine-aspartic; PEG-MAL = poly(ethylene glycol)-maleimide; PASP = polyaspartic acid. **(b)** Decay-corrected whole-body coronal PET images of human U87MG tumor-bearing nude mouse at 1, 4, and 21 h after injection of ^{64}Cu-DOTA-IO, ^{64}Cu-DOTA-IO-RGD, or ^{64}Cu-DOTA-IO-RGD (left). Time-activity curves of U87MG tumors after injection of ^{64}Cu-DOTA-IO, ^{64}Cu-DOTA-IO-RGD, or ^{64}Cu-DOTA-IO-RGD with blocking dose of c(RGDyK) (*n* = 3/group) (right). **(c)** T2-weighted MR images of U87MG tumor-bearing nude mice before injection of IO nanoparticles (c-1 and c-5) and at 4 h after tail-vein injection of DOTA-IO (c-2 and c-6), DOTA-IO-RGD (c-3 and c-7), and DOTA-IO-RGD with blocking dose of c(RGDyK) (c-4 and c-8). **(d)** Prussian blue-stained U87MG tumor, liver, and spleen sections after injection of ^{64}Cu-DOTA-IO-RGD, ^{64}Cu-DOTA-IO, and ^{64}Cu-DOTA-IO-RGD with blocking dose of c(RGDyK). IO was stained as blue spots in figure (magnification, 200x). (Adapted with permission from ref. 82. Copyright (2008) The Society of Nuclear Medicine and Molecular Imaging).

such dual-modal imaging can overcome the limits of imaging quality. Especially useful for imaging applications, quantum dots (QDs) are nanometer-sized inorganic fluorescent semiconductor crystals with excellent optical properties such as high quantum yield and molecular extinction coefficients, along with low photo-bleaching and composition-tunable absorption and emission spectra ranging from ultraviolet to near-infrared [45,85,86]. By introducing radionuclides using a chelating agent on the surface of QDs, PET (or SPECT) and NIRF dual-modal imaging techniques can be used. Cai et al. successfully synthesized QDs-based PET/NIRF imaging probes by conjugating QDs with cyclic RGD peptide for targeting and imaging tumors (integrin $\alpha_v\beta_3$ expressing U87MG tumor xenografts) [54] (Figure 6). In that work, DOTA was introduced as a chelating agent for incorporating radionuclides, with ^{64}Cu and CdTe QDs used for NIRF imaging. These dual-modal imaging probes showed excellent tumor uptake behavior, and a linear correlation between PET and NIRF signal intensities was confirmed. Furthermore, QD-based PET/NIRF imaging probes significantly reduced the potential toxicity and overcame the tissue penetration limit of optical imaging. In another study, Liang et al., reported SPECT/NIRF tumor imaging probes using streptavidin coated nanoparticles [87]. These streptavidin nanoparticles were conjugated with three types of molecules: biotinylated anti-Her2 Herceptin antibodiesto target a SUM190 (Her2+) tumor, biotinylated DOTA chelating agents for labeling of radionuclides (^{111}In), and biotinylated Cy5.5 fluorophores for NIRF imaging. The SPECT/NIRF imaging displayed high tumor accumulation and strong tumor-to-normal tissue contrast, and the specific tumor accumulation of radioactivity at 40 h was 21 ID%/g, which denoted a higher accumulation

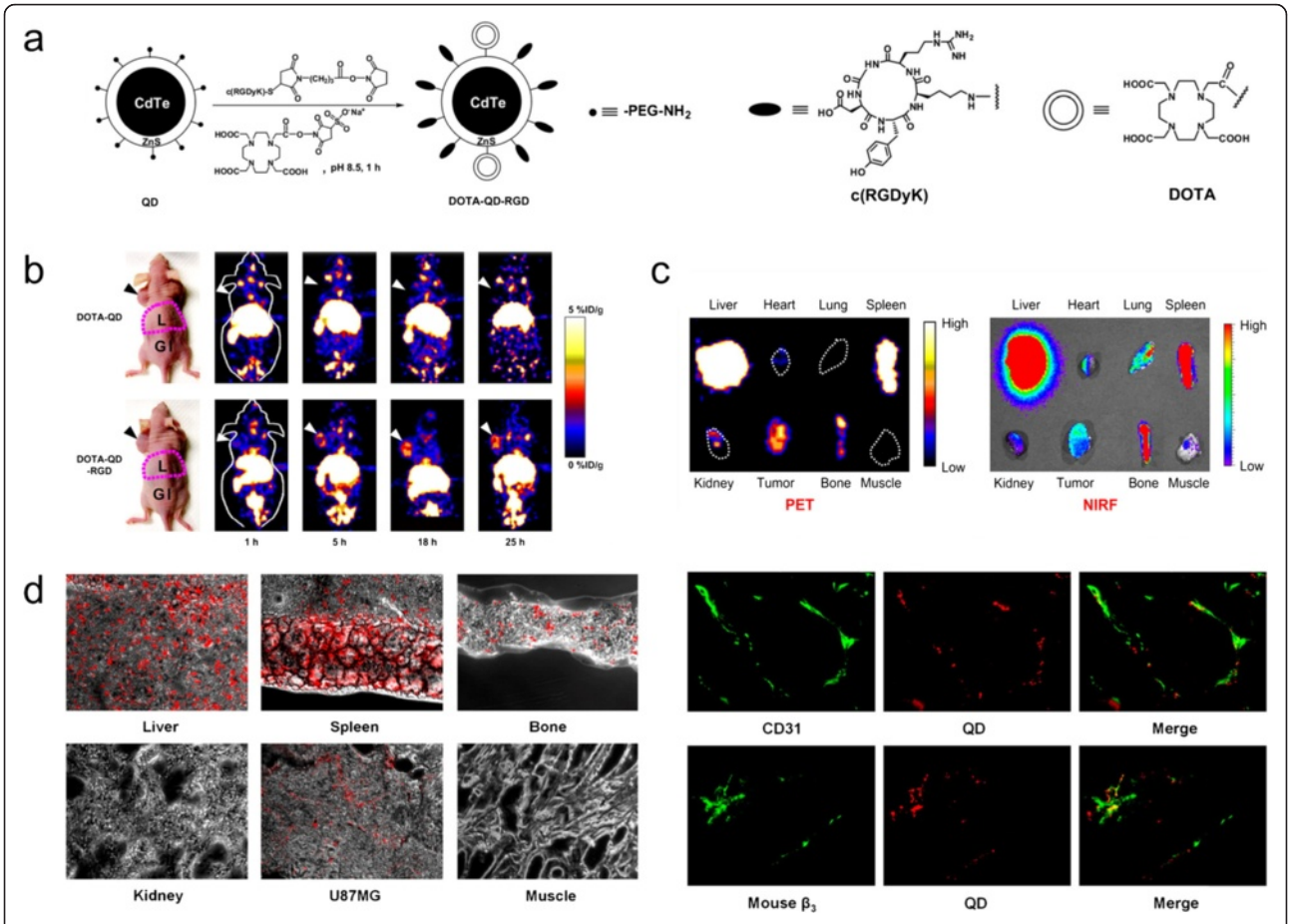

Figure 6 PET(SPECT)/optical imaging. (a) Preparation of dual functional PET/NIRF probe DOTA-QD-RGD. DOTA = 1,4,7,10-tetraazacyclododecane-*N*,*N*′,*N*″,*N*‴-tetraacetic acid; QD = Quantum Dot; RGD = arginine-glycine-aspartic acid; PEG = polyethylene glycol. **(b)** *In vivo* PET of mice bearing U87MG tumor with dual functional PET/NIRF probe. Whole-body coronal PET images of mice at 1, 5, 18, and 25 h after injection of ^{64}Cu-labeled DOTA -QD or DOTA -QD -RGD. Arrows indicate tumors. GI = gastrointestinal tract; L = liver. **(c)** *Ex vivo* PET (left) and NIRF (right) image of harvested tissues at 5 h after injection of ^{64}Cu-labeled DOTA-QD-RGD. **(d)** Histologic analysis of DOTA-QD-RGD distribution in U87MG tumors and other tissues. Overlay of bright-field and QD fluorescence images of frozen tissue slices (5 μm thick) (left). Immunofluorescence staining (CD31 and mouse β_3) of frozen U87MG tumor slices from mice injected with ^{64}Cu-labeled DOTA-QD-RGD (right). (Adapted with permission from ref. 54. Copyright (2010) The Society of Nuclear Medicine and Molecular Imaging).

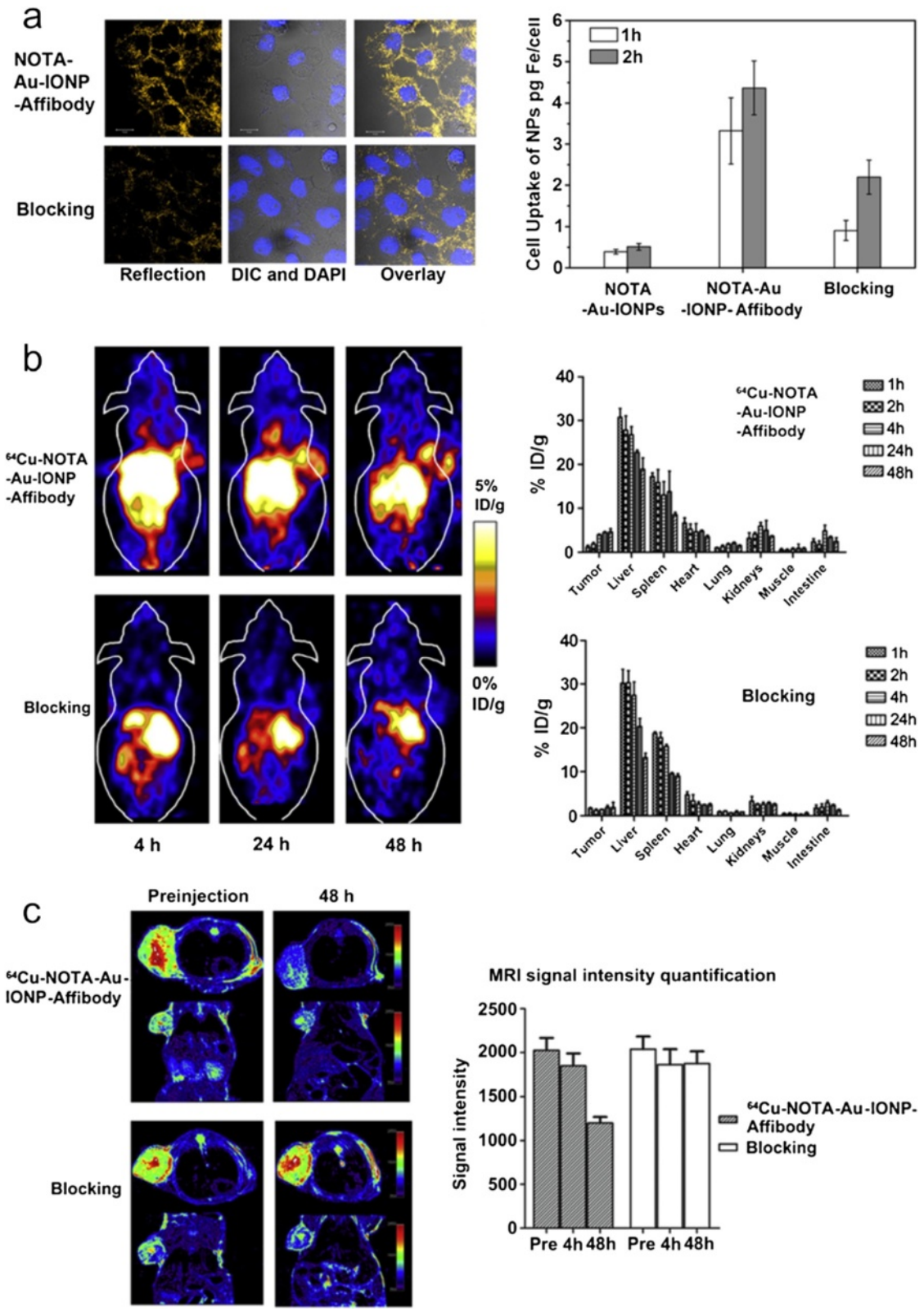

Figure 7 (See legend on next page.)

(See figure on previous page.)
Figure 7 PET(SPECT)/MR/optical imaging. (a) Reflection and confocal images of A431 cells labeled with NOTA-Au-IONP-Affibody (left). NOTA = 1,4,7-triazacyclononane-1,4,7-triacetic acid; IONP = iron oxide nanoparticle. Quantification analysis of the cellular uptake with NOTA-Au-IONP, NOTA-Au-IONP-Affibody, and Affibody blocked NOTA-Au-IONP-Affibody in A431 cells after incubation (right). **(b)** *In vivo* decay-corrected whole-body coronal PET images of A431 tumor bearing mice (n = 3/group) (left). Quantitative analysis of PET images of tissues and organs (right). **(c)** *In vivo* T2-weighted MR images of A431 tumor bearing mice (left). Quantification of MRI signal intensity before and at 4 h and 48 h after injection of ^{64}Cu-NOTA-Au-IONP-Affibody and Affibody (right). (Adapted with permission from ref. 89. Copyright (2013) Elsevier).

than all other tissues, including those from the liver, heart, kidney, spleen, and muscle.

2.3.3 PET(SPECT)/MR/optical imaging

With the easily modifiable surface chemistry of nanoparticles, two or even more imaging labels can be introduced to a single nanoparticle with multiple linking agents (ligands) or direct-incorporation. With this expansive nature, nanoprobes can be designed for imaging modalities beyond two modes. Recently, such multifunctional imaging probes containing three different imaging modalities have been developed [88-91]. Park et al. successfully synthesized optical/PET/MR hybrid nanoprobes by conjugating a PET radionuclide (^{124}I) to an MRI probe (SPIONPs) [88]. These optical/PET/MR hybrid nanoprobes could screen lymph node metastasis with high sensitivity using optical imaging and then provide accurate 3D visualization of accumulated nanoprobes with detailed anatomical information using PET and MR imaging. Yang et al. also provided Affibody modified and radiolabeled Au-IO hetero-nanostructures for tumor optical/PET/MR-based multi-modal imaging probes using NOTA as a chelating agent for a ^{64}Cu radionuclide [89] (Figure 7). Such hetero-nanoprobes can show surface-specific modification of both targeting molecules (anti-EGFR Affibody protein) and PET imaging reporters (^{64}Cu) with high efficiency and reliability. The NOTA-Au-IONP-Affibody was very stable in 10% fetal bovine serum in PBS at 37°C for 48 h with little variation of particle size. By taking advantage of the plasmonic properties of AuNPs imaging, the NOTA-Au-IONP-Affibody could be used for cell assays with a scanning confocal microscope. For both PET and MR imaging, *in vitro* and *in vivo* studies showed high specificity, sensitivity, and excellent tumor contrast in human EGFR-expressing cells and tumors. Xie et al. functionalized dopamine to the surface of IONPs for facile encapsulation into human serum albumin (HSA) matrices, and labeled both ^{64}Cu-DOTA and Cy5.5 onto the HSA coated IONPs to enable PET/MR/NIRF multi-modal imaging [90]. *In vivo* PET/NIRF/MR tri-modality imaging, and *ex vivo* analyses, indicated that the ^{64}Cu-DOTA and Cy5.5 labeled HSA-IONPs have a good retention and high extravasation rates at the tumor site. Impressively, HSA-IONPs showed a prolonged circulation half-life, high accumulation in lesions, and low uptake of the particles by macrophages due to compact HSA coating. Unlike IONP-based MR imaging, Lee et al. reported RGD peptide-conjugated multi-modal Yb^{3+}/Er^{3+} co-doped $NaGdF_4$ upconversion nanophosphors for PET/MR/optical imaging of tumor angiogenesis [91]. In their report, Gd, a component of nanophosphors, was used as a T_1-weighted MRI contrast agent rather than IONPs. The assembly was radiolabeled with ^{124}I and conjugated with a tyrosine residue of dimeric cyclic RGDyk peptide targeting integrin $\alpha v\beta_3$, and Yb^{3+}/Er^{3+} was doped to enable fluorescence imaging. These multi-modal imaging techniques are beneficial for real clinical applications, such as early diagnosis, by maximizing detection at different levels. However, the synthesis of nanostructures for multimodal imaging can present challenges of its own, as steps in synthesizing one mode may interfere with another. Thus, the synthetic procedure must be planned carefully to achieve ideal activity from each imaging mode in the finished product [92].

3 Conclusions

A variety of nanostructures have been utilized for *in vivo* diagnostic and therapeutic agents. In this review, nanostructures labeled with radionuclides were introduced for *in vivo* tumor imaging. Although many chelating agents have been used to incorporate radionuclides into nanostructures for molecular imaging, there is a need to develop radionuclide labeling strategies free of chelating agents for *in vivo* nuclear molecular imaging accuracy while maintaining biocompatibility. Moreover, multimodality molecular imaging should be used to overcome limitations in the imaging quality of a single modality. Although multimodality tumor imaging techniques have been developed remarkably over the past decade, most of those techniques have not moved beyond basic research. More effort should focus on the clinical applications of nanostructures for multimodality imaging. Given the insights that these allow into different physiological properties of tumors and disease, these nanostructures will likely to generate advancements in diagnosis and therapy across a wide range of medical fields.

Competing interests

The authors declare that they have no competing interests.

Authors' contributions

All authors have contributed to the writing of the manuscript. All authors read and approved the final manuscript.

Acknowledgement
J.-M.N. was supported by the National Research Foundation of Korea (2011-0018198) and the Pioneer Research Center Program (2012-0009586) through the NRF of Korea funded by the Ministry of Science, ICT, and Future Planning. K.W.K. was supported by National Nuclear R&D Programs through the National Research Foundation of Korea (NRF) funded by the Ministry of Education, Science and Technology (NRF-2012M2A2A7014020).

Author details
[1]Department of Chemistry, Seoul National University, Seoul 151-747, Republic of Korea. [2]Department of Nuclear Medicine, Seoul National University College of Medicine, Seoul 110-744, Republic of Korea.

Received: 3 November 2014 Accepted: 10 November 2014
Published online: 13 May 2015

References

1. TF Massoud, SS Gambhir, Genes Dev. **17**, 545 (2003)
2. M Shokeen, CJ Anderson, Acc. Chem. Res. **42**, 832 (2009)
3. R Weissleder, Science **312**, 1168 (2006)
4. HR Herschman, Science **302**, 605 (2003)
5. MA Pysz, SS Gambhir, JK Willmann, Clin. Radiol. **65**, 500 (2010)
6. M Mahmoudi, V Serpooshan, S Laurent, Nanoscale **3**, 3007 (2011)
7. SS Gambhir, Nat. Rev. Cancer **2**, 683 (2002)
8. LW Dobrucki, AJ Sinusas, Nat. Rev. Cardiol. **7**, 38 (2009)
9. AF Chatziioannou, Proc. Am. Thorac. Soc. **2**, 533 (2005)
10. ME Phelps, J. Nucl. Med. **41**, 661 (2000)
11. C Anderson, J Connett, S Schwarz, P Rocque, L Guo, G Philpott, K Zinn, C Meares, M Welch, J. Nucl. Med. Allied Sci. **33**, 1685 (1992)
12. AM Wu, PJ Yazaki, T S-w, K Nguyen, A-L Anderson, DW McCarthy, MJ Welch, JE Shively, LE Williams, AA Raubitschek, Proc. Natl. Acad. Sci. U. S. A **97**, 8495 (2000)
13. X Chen, Y Hou, M Tohme, R Park, V Khankaldyyan, I Gonzales-Gomez, JR Bading, WE Laug, PS Conti, J. Nucl. Med **45**, 1776 (2004)
14. DS Wilbur, Bioconj. Chem. **3**, 433 (1992)
15. A Roivainen, T Tolvanen, S Salomäki, G Lendvai, I Velikyan, P Numminen, M Välilä, H Sipilä, M Bergström, P Härkönen, J. Nucl. Med. **45**, 347 (2004)
16. E Mishani, G Abourbeh, Curr. Top. Med. Chem. **7**, 1755 (2007)
17. H Hong, Y Zhang, JT Sun, WB Cai, Nano. Today **4**, 399 (2009)
18. H Xie, ZJ Wang, A Bao, B Goins, WT Phillips, Int. J. Pharm. **395**, 324 (2010)
19. Y Wang, Y Liu, H Luehmann, X Xia, P Brown, C Jarreau, M Welch, Y Xia, ACS Nano. **6**, 5880 (2012)
20. Z Liu, W Cai, L He, N Nakayama, K Chen, X Sun, X Chen, H Dai, Nat. Nanotechnol. **2**, 47 (2006)
21. H Hong, K Yang, Y Zhang, JW Engle, L Feng, Y Yang, TR Nayak, S Goel, J Bean, CP Theuer, Acs Nano **6**, 2361 (2012)
22. B Cornelissen, S Able, V Kersemans, PA Waghorn, S Myhra, K Jurkshat, A Crossley, KA Vallis, Biomaterials **34**, 1146 (2013)
23. JW Seo, H Zhang, DL Kukis, CF Meares, KW Ferrara, Bioconj. Chem. **19**, 2577 (2008)
24. AL Petersen, T Binderup, P Rasmussen, JR Henriksen, DR Elema, A Kjær, TL Andresen, Biomaterials **32**, 2334 (2011)
25. CA Boswell, XK Sun, WJ Niu, GR Weisman, EH Wong, AL Rheingold, CJ Anderson, J. Med. Chem. **47**, 1465 (2004)
26. MS Cooper, MT Ma, K Sunassee, KP Shaw, JD Williams, RL Paul, PS Donnelly, PJ Blower, Bioconj. Chem. **23**, 1029 (2012)
27. KP Maresca, SM Hillier, FJ Femia, CN Zimmerman, MK Levadala, SR Banerjee, J Hicks, C Sundararajan, J Valliant, J Zubieta, WC Eckelman, JL Joyal, JW Babich, Bioconj. Chem. **20**, 1625 (2009)
28. M Zhou, R Zhang, M Huang, W Lu, S Song, MP Melancon, M Tian, D Liang, C Li, J. Am. Chem. Soc. **132**, 15351 (2010)
29. KC Black, Y Wang, HP Luehmann, X Cai, W Xing, B Pang, Y Zhao, CS Cutler, LV Wang, Y Liu, ACS Nano **8**, 4385 (2014)
30. YF Zhao, D Sultan, L Detering, SH Cho, GR Sun, R Pierce, KL Wooley, YJ Liu, Angew. Chem. Int. Ed. **53**, 156 (2014)
31. X Sun, X Huang, X Yan, Y Wang, J Guo, O Jacobson, D Liu, LP Szajek, W Zhu, G Niu, ACS Nano **8**, 8438 (2014)
32. YH Kim, J Jeon, SH Hong, WK Rhim, YS Lee, H Youn, JK Chung, MC Lee, DS Lee, KW Kang, JM Nam, Small **7**, 2052 (2011)
33. R Weissleder, U Mahmood, Radiology **219**, 316 (2001)
34. Y Xing, J Zhao, PS Conti, K Chen, Theranostics **4**, 290 (2014)
35. M Petrik, H Haas, G Dobrozemsky, C Lass-Flörl, A Helbok, M Blatzer, H Dietrich, C Decristoforo, J. Nucl. Med. **51**, 639 (2010)
36. W Chen, T Cloughesy, N Kamdar, N Satyamurthy, M Bergsneider, L Liau, P Mischel, J Czernin, ME Phelps, DH Silverman, J. Nucl. Med **46**, 945 (2005)
37. RJ Jaszczak, KL Greer, CE Floyd Jr, CC Harris, RE Coleman, J. Nucl. Med. **25**, 893 (1984)
38. J Cheon, J-H Lee, Acc. Chem. Res. **41**, 1630 (2008)
39. DA Giljohann, CA Mirkin, Nature **462**, 461 (2009)
40. H Goesmann, C Feldmann, Angew. Chem. Int. Ed **49**, 1362 (2010)
41. J Kim, JE Lee, SH Lee, JH Yu, JH Lee, TG Park, T Hyeon, Adv. Mater. **20**, 478 (2008)
42. T Lammers, S Aime, WE Hennink, G Storm, F Kiessling, Acc. Chem. Res. **44**, 1029 (2011)
43. S-D Li, L Huang, Mol. Pharm. **5**, 496 (2008)
44. Y Liu, MJ Welch, Bioconj. Chem. **23**, 671 (2012)
45. X Michalet, FF Pinaud, LA Bentolila, JM Tsay, S Doose, JJ Li, G Sundaresan, AM Wu, SS Gambhir, S Weiss, Science **307**, 538 (2005)
46. R Mout, DF Moyano, S Rana, VM Rotello, Chem. Soc. Rev **41**, 2539 (2012)
47. X Sun, Z Liu, K Welsher, JT Robinson, A Goodwin, S Zaric, H Dai, Nano Res. **1**, 203 (2008)
48. Y Xia, Nat. Mater. **7**, 758 (2008)
49. J Fang, H Nakamura, H Maeda, Adv. Drug Del. Rev. **63**, 136 (2011)
50. F Alexis, E Pridgen, LK Molnar, OC Farokhzad, Mol. Pharm. **5**, 505 (2008)
51. G Zhang, Z Yang, W Lu, R Zhang, Q Huang, M Tian, L Li, D Liang, C Li, Biomaterials **30**, 1928 (2009)
52. MR McDevitt, D Chattopadhyay, JS Jaggi, RD Finn, PB Zanzonico, C Villa, D Rey, J Mendenhall, CA Batt, JT Njardarson, PLoS One **2**, e907 (2007)
53. ML Schipper, Z Cheng, SW Lee, LA Bentolila, G Iyer, JH Rao, XY Chen, AM Wul, S Weiss, SS Gambhirl, J. Nucl. Med. **48**, 1511 (2007)
54. WB Cai, K Chen, ZB Li, SS Gambhir, XY Chen, J. Nucl. Med. **48**, 1862 (2007)
55. JD Correia, A Paulo, PD Raposinho, I Santos, Dalton Trans. **40**, 6144 (2011)
56. A Bolton, W Hunter, Biochem. J. **133**, 529 (1973)
57. AM Alkilany, CJ Murphy, J. Nanopart. Res. **12**, 2313 (2010)
58. CM Cobley, J Chen, EC Cho, LV Wang, Y Xia, Chem. Soc. Rev. **40**, 44 (2011)
59. CJ Murphy, AM Gole, JW Stone, PN Sisco, AM Alkilany, EC Goldsmith, SC Baxter, Acc. Chem. Res. **41**, 1721 (2008)
60. WK Rhim, JS Kim, JM Nam, Small **4**, 1651 (2008)
61. K Balasubramanian, M Burghard, Small **1**, 180 (2005)
62. A De La Zerda, C Zavaleta, S Keren, S Vaithilingam, S Bodapati, Z Liu, J Levi, BR Smith, T-J Ma, O Oralkan, Nat. Nanotechnol. **3**, 557 (2008)
63. H Hong, T Gao, W Cai, Nano Today **4**, 252 (2009)
64. K Kostarelos, A Bianco, M Prato, Nat. Nanotechnol **4**, 627 (2009)
65. L Feng, Z Liu, Nanomedicine **6**, 317 (2011)
66. B Tian, C Wang, S Zhang, L Feng, Z Liu, Acs Nano **5**, 7000 (2011)
67. K-H Liao, Y-S Lin, CW Macosko, CL Haynes, ACS Appl. Mater. Interfaces **3**, 2607 (2011)
68. K Yang, J Wan, S Zhang, Y Zhang, S-T Lee, Z Liu, ACS Nano **5**, 516 (2010)
69. H Hong, Y Zhang, JW Engle, TR Nayak, CP Theuer, RJ Nickles, TE Barnhart, W Cai, Biomaterials **33**, 4147 (2012)
70. WT Al-Jamal, K Kostarelos, Acc. Chem. Res. **44**, 1094 (2011)
71. PL Felgner, G Ringold, Nature **337**, 387 (1989)
72. VP Torchilin, Nat. Rev. Drug Discov. **4**, 145 (2005)
73. OC Farokhzad, R Langer, Adv. Drug Del. Rev. **58**, 1456 (2006)
74. ML Schipper, G Iyer, AL Koh, Z Cheng, Y Ebenstein, A Aharoni, S Keren, LA Bentolila, JQ Li, JH Rao, XY Chen, U Banin, AM Wu, R Sinclair, S Weiss, SS Gambhir, Small **5**, 126 (2009)
75. LA Bass, M Wang, MJ Welch, CJ Anderson, Bioconj. Chem. **11**, 527 (2000)
76. N Gibson, U Holzwarth, K Abbas, F Simonelli, J Kozempel, I Cydzik, G Cotogno, A Bulgheroni, D Gilliland, J Ponti, F Franchini, P Marmorato, H Stamm, W Kreyling, A Wenk, M Semmler-Behnke, S Buono, L Maciocco, N Burgio, Arch. Toxicol. **85**, 751 (2011)
77. WL Cheng, SJ Dong, EK Wang, Angew. Chem. Int. Ed. **42**, 449 (2003)
78. X Shao, A Agarwal, JR Rajian, NA Kotov, X Wang, Nanotechnology **22**, 135102 (2011)
79. S Singh, R Pasricha, UM Bhatta, PV Satyam, M Sastry, BLV Prasad, J. Mater. Chem. **17**, 1614 (2007)
80. AP Pathak, B Gimi, K Glunde, E Ackerstaff, D Artemov, ZM Bhujwalla, Methods Enzymol. **386**, 1 (2004)
81. Y Ling, K Wei, Y Luo, X Gao, SZ Zhong, Biomaterials **32**, 7139 (2011)
82. HY Lee, Z Li, K Chen, AR Hsu, CJ Xu, J Xie, SH Sun, XY Chen, J. Nucl. Med. **49**, 1371 (2008)

83. JS Choi, JC Park, H Nah, S Woo, J Oh, KM Kim, GJ Cheon, Y Chang, J Yoo, J Cheon, Angew. Chem. Int. Ed. **47**, 6259 (2008)
84. R Misri, D Meier, AC Yung, P Kozlowski, UO Hafeli, Nanomed.-Nanotechnol. Biol. Med. **8**, 1007 (2012)
85. WB Cai, AR Hsu, ZB Li, XY Chen, Nanoscale Res. Lett. **2**, 265 (2007)
86. IL Medintz, HT Uyeda, ER Goldman, H Mattoussi, Nat. Mater. **4**, 435 (2005)
87. M Liang, X Liu, D Cheng, G Liu, S Dou, Y Wang, M Rusckowski, DJ Hnatowich, Bioconj. Chem. **21**, 1385 (2010)
88. JC Park, MK Yu, G Il An, SI Park, J Oh, HJ Kim, JH Kim, EK Wang, IH Hong, YS Ha, TH Choi, KS Jeong, Y Chang, MJ Welch, S Jon, J Yoo, Small **6**, 2863 (2010)
89. M Yang, K Cheng, SB Qi, HG Liu, YX Jiang, H Jiang, JB Li, K Chen, HM Zhang, Z Cheng, Biomaterials **34**, 2796 (2013)
90. J Xie, K Chen, J Huang, S Lee, J Wang, J Gao, X Li, X Chen, Biomaterials **31**, 3016 (2010)
91. J Lee, TS Lee, J Ryu, S Hong, M Kang, K Im, JH Kang, SM Lim, S Park, R Song, J. Nucl. Med. **54**, 96 (2013)
92. BP Joshi, TD Wang, Cancers (Basel) **2**, 1251 (2010)